Power absorption of a two-body heaving wave energy converter considering different control and power take-off systems

Xiaochen Dong[a]; Zhen Gao[b]; Demin Li[a]; Shuting Huang[e]; Hongda Shi[a, c, d*]

[a] Department of Ocean Engineering, College of Engineering, Ocean University of China, Qingdao, 266100, China

[b] Department of Marine Technology and Centre for Autonomous Marine Operations and Systems (AMOS), Norwegian University of Science and Technology (NTNU), Trondheim, 7491, Norway

[c] Shandong Provincial Key Laboratory of Ocean Engineering, Ocean University of China, Qingdao, 266100, China

[d] Qingdao Municipal Key Laboratory of Ocean Renewable Energy, Ocean University of China, Qingdao, 266100, China

[e] Institute of Marine Science and Technology, Shandong University, Qingdao, 266237, China

[*] Corresponding author. Department of Ocean Engineering, College of Engineering, Ocean University of China, Qingdao, 266100, China

E-mail address: Hongda.shi@ouc.edu.cn (Hongda Shi).

Abstract

This study proposed a wave power system with two coaxial floating cylinders of different diameters and drafts. Wavebob's conceptual design has been adopted in the wave power system. In this study, a basic analysis of the wave energy extraction by the relative motion between two floats is presented. The maximum power absorption was studied theoretically under regular wave conditions, and the effects of both linear and constant damping forces on the power take-off (PTO) were investigated. A set of dynamic equations describing the floats' displacement under regular waves and different PTOs are established. A time-domain numerical model is developed, considering the PTO parameter and viscous damping, and the optimal PTO damping and output power are obtained. With the analysis of estimating the maximum power absorption, a new estimation method called Power Capture Function (PCF) is proposed and constructed, which can be used to predict the power capture under both linear and constant PTO forces. Based on this, energy extraction is analyzed and optimized. Finally, the performance characteristics of the two-body power system are concluded.

Key words: two-body heaving wave energy converter, power capture function, power take-off

1 Introduction

Marine renewable energy is a promising alternative to fossil fuels because of its broad distribution and high density. Wave energy, as one of the marine renewables, plays an important role because of its huge reserves. Among the various wave energy converters (WECs), point absorbers are widely used for their adaptability to wave conditions. The basic topological model of these WECs lies in a two-body device, which utilizes the relative heave motion between two floats or with a fixed reference to capture energy through a power take-off (PTO) system. It has only one direction in the movement (i.e., the heave direction), which could be considered as the axial motion and along which the wave energy is extracted. Consequently, the study on the two-body heaving system is very important, and the results obtained would have a wide impact on the design of WECs that harness wave energy by relative motions. To date, some designs fix one of the floats by a mooring system and cause the other float to oscillate with waves; therefore, only one degree of freedom (DOF) works indeed (Son et al., 2016), while others allow both floats to move independently, using the reaction of one float against the other (Beatty et al., 2019). Because the double-float system is adaptable to deep water, it has the potential for commercialization, while the hydrodynamic interference between the moving bodies must be well studied beforehand. As some studies have examined the difference between one and two DOF systems (Wang et al., 2016), this study focuses on the two-DOF system, and the one-DOF system is used for comparison.

First, the hydrodynamic coefficients, namely, the added mass, radiation damping, and excitation force, are solved in many ways. The validity of these coefficients is the foundation of the hydrodynamic analysis. The methods of separation of variables and matched eigenfunction expansion are always used to compute the coefficients (Chau and Yeung, 2012). Since the small gap between floats greatly affects the solution, a semi-analytical solution is proposed to solve the hydrodynamic radiation problem (Mavrakos, 2004). Researchers have used the boundary element method (Zhang et al., 2019), the finite element method (Yang et al., 2018), and other numerical methods to solve hydrodynamic issues. Commercial software such as Ansys-Aqwa (Al Shami et al., 2019), WAMIT (Kalidoss and Banerjee, 2019), and OrcaFlex (Lewis et al., 2012) are also used to provide a fine description of the WEC performance. To overcome the shortcomings of the ideal fluid hypothesis and to improve the accuracy of the results, the nonlinear factor and viscous effect are considered. The nonlinear effects of the hydrostatic force (Ji et al., 2020), drag force (Xu et al., 2019), and mooring force (Amann et al., 2015) will suppress the motion of the WEC, making the results closer to reality. With respect to viscous fluid, a computational fluid dynamics (CFD) method is proposed. One of the CFD methods, the Reynolds-averaged Navier–Stokes (RANS) method is wildly used to simulate the performance of the WEC (Yu and Li, 2013). It can model complex hydrodynamic interactions, such as wave breaking and overtopping. Furthermore, the overset mesh has been shown to better describe a moving object (Chen et al., 2019). On the other hand, some nonlinear terms are not so crucial that they can be linearized to improve the simulation efficiency (Tan et al., 2020). In this paper, as the configuration of the WEC, the viscous effect is considered but linearized to make the result convincing. The reliability and accuracy of linearization have also been proven.

The power absorption of the WEC is the key indicator, but it is affected by many factors. A range of efforts has been made to optimize the power capture of the two-body heaving WEC. The geometrical parameters of the float, which influence the hydrodynamic performance and efficiency, have been studied (Berenjkoob et al., 2019a). It was found that the device with a conical tube can improve the power absorption (Kurniawan et al. 2019). Moreover, the optimization algorithm is also applied in dimensioning the WEC, such as the differential evolutionary algorithms (Blanco et al., 2019). The configuration of the mooring system also plays an important role in the performance of WECs (Berenjkoob et al., 2019b). In addition, arranging a wave farm is a necessary way to harness wave energy eventually (Ji et al., 2019). In this paper, a basic coaxial structure based on Wavebob's conceptual design is proposed to expose the power absorption of a two-body device. Furthermore, a new estimation method is proposed to obtain the optimal power absorption in a simple and effective manner. Compared with the existing methods, the new method saves time and effort.

When evaluating the performance of a WEC, not only the peak capture is concerned, but also the capture width matters; however, the two-body heaving WEC has the advantage of a wider capture frequency domain. Normally, the natural frequency of the WEC should be determined in accordance with the objective sea conditions. Furthermore, the power capture can be improved productively by adjusting the PTO damping force. There are some typical PTOs employed in two-body heaving WECs, such as linear generators (Elwood et al., 2010), hydraulic systems (Negandari et al., 2018), and electromechanical systems (Dai et al., 2017). A linear generator has a simple structure that can minimize mechanical loss and provide a linear damping force (Phung et al., 2019). A primary excitation fully superconducting linear generator provides a larger output power (Huang et al., 2019). For a hydraulic system, the piston area, volume flow rate, and rotation velocity of the motor affect the power capture efficiency (Kalidoss and Banerjee, 2019). In an electromechanical system, the gearbox and resistance of the generator determine the power capture (Castro and Chiang, 2020). In addition, the control strategy plays an important role in the energy extraction. The active control of the generator damping and stiffness is an effective way to achieve a wider frequency range (Jin et al., 2019). Most studies consider one certain PTO damping force, which are predominantly linear, while, in this paper, the optimal conditions are addressed in both linear and constant PTO systems, and a new estimation formula which is suitable for both systems is explored. The theoretical model has been validated via a physical test from the reference laboratory (Dong et al., 2021), and the results are of general importance to all the WECs that utilize the relative motion. The passive control has only a PTO damping term, whereas the active control has both a PTO stiffness term and a PTO damping term. The passive control is the optimal control when only the PTO damping is considered. It is the sub-domain optimal control. In terms of the active control, the stiffness and damping coefficients can be adjusted to be consistent with the external environment. Hence, the optimal absorbed power with active control is always larger than that of the passive control. In addition, the optimal power under constant PTO, which depends on the existence of the accumulator, is also discussed. Different control strategies and PTO systems increase the diversity of the power absorption. In the theoretical analysis, the optimal condition is explored by derivation, whereas the optimal damping is determined through parameter sweeping in the numerical simulation. The credibility of the results is validated through comparison.

The remainder of this paper is organized as follows. Section 2 illustrates the dynamic analysis of the two-body heaving WEC, considering both linear and constant PTO damping forces. The analysis models are validated against the published research results. Section 3 discusses the power capture characteristics of the system, including the relations between the key parameters and the power capture. Section 4 proposes a new estimation formula of the power capture function (PCF), which can be used to predict the optimal PTO and power absorption of the WEC. The final section presents the conclusions of this study.

2 Dynamic analysis of a two-body heaving wave energy converter

2.1 Theoretical model setup

To describe the relative motion and power capture of the floats under waves, a system that includes two coaxial cylinders that heave along the same vertical axis is considered. The outer float is an annular rigid body, whereas the inner float is a rigid cylinder, as shown in Fig. 1. The outer and inner radii of the outer float are R_1 and r_1, respectively. The draft of the outer float is D_1. The radius of the inner float is R_2, and the draft is D_2. These two floats are connected through a PTO system, and energy is captured by the relative motion with the water depth d. A Cartesian coordinate system O-xyz is defined with the origin at the still water level and the z-axis positive upward. The fluid is incompressible, and the movement of water particles is irrotational. Compared with the incident wave length, the diameters of the floats are sufficiently small. Therefore, the linear wave theory is applied here. Based on the above assumption, the governing equation of the two-body heaving WEC is described as follows.

$$\begin{cases} \left[m_1 + A_{11}(\infty)\right]\ddot{z}_1(t) + A_{12}(\infty)\ddot{z}_2(t) + k_{11}(t)*\dot{z}_1(t) + k_{12}(t)*\dot{z}_2(t) + B_{vis1}\dot{z}_1(t) + C_1 z_1(t) = f_{e1}(t) + f_{PTO}(t) \\ \left[m_2 + A_{22}(\infty)\right]\ddot{z}_2(t) + A_{21}(\infty)\ddot{z}_1(t) + k_{22}(t)*\dot{z}_2(t) + k_{21}(t)*\dot{z}_1(t) + B_{vis2}\dot{z}_2(t) + \left(C_2 + K_m\right) z_2(t) = f_{e2}(t) - f_{PTO}(t) \end{cases} \tag{1}$$

where, subscript 1 denotes the outer float, and 2 represents the inner one, respectively; m_i stands for the mass of a float; C_i is the restoring force coefficient; K_m is the mooring stiffness; B_{visi} is the linearized viscous damping coefficient; f_{ei} is the excitation force on the float; z_i is the float's displacement, where $\dot{z}_i$ and $\ddot{z}_i$ are the velocity and the acceleration; and the symbol (*) denotes the operation of convolution. Furthermore, $k_{iq}(t)$ is the radiation-force impulse-response function, which is the inverse Fourier transform of

$$K_{iq}(\omega) = j\omega[A_{iq}(\omega) - A_{iq}(\infty)] + B_{iq}(\omega) \tag{2}$$

where $B_{iq}(\omega)$ is the radiation damping coefficient, $A_{iq}(\omega)$ is the added mass, and $A_{iq}(\infty)$ is the added mass when $\omega = \infty$.

The incident wave power per unit width is expressed as

$$P_{wave} = \frac{\rho g H^2 L}{16T}(1 + \frac{2kd}{\sinh(2kd)}) \tag{3}$$

The capture width ratio (CWR) is

$$CWR = \frac{P}{2R_1 P_{wave}} \tag{4}$$

where ρ is the water density, g depicts the gravitational acceleration, H is the wave height, L represents wave length, T is the wave period, k denotes the wave number, and P is the power captured by the WEC.

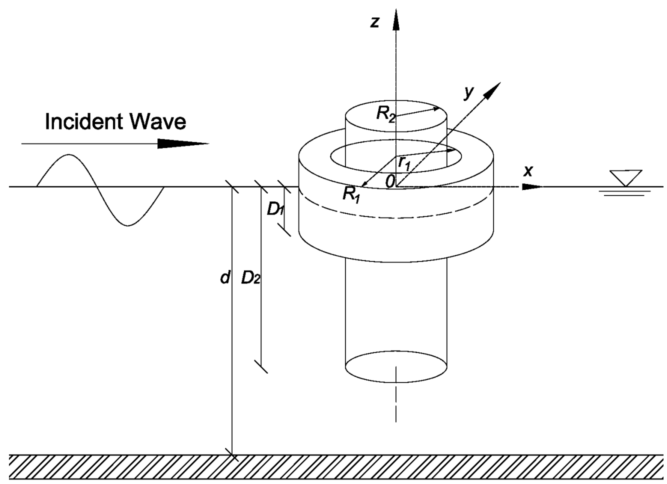

Fig. 1. Schematic of the two-body heaving WEC.

2.2 Power absorption under the linear PTO damping

As one of the descriptions of Eq. (1), the PTO force is assumed to be linear and written as $f_{PTO}(t) = -K(z_1 - z_2) - B(\dot{z}_1 - \dot{z}_2)$, where B is the linear PTO damping coefficient, and K is the stiffness coefficient. Because the system is suspended in water, K should be positive or equal to zero (Liang and Zuo, 2017). The incident wave is defined as the frequency ω_0 and the unit wave amplitude. Assuming that the phase angles between the incident wave and body motion, the excitation force are φ_1, φ_2, φ_3, and φ_4. The heave motions and excitation forces in equation (1) can be expressed as, $z_1(t) = \mathrm{Re}(Z_1 e^{j\varphi_1} e^{j\omega_0 t}) = \mathrm{Re}(\hat{Z}_1 e^{j\omega_0 t})$, $z_2(t) = \mathrm{Re}(Z_2 e^{j\varphi_2} e^{j\omega_0 t}) = \mathrm{Re}(\hat{Z}_2 e^{j\omega_0 t})$, $f_{e1}(t) = \mathrm{Re}(F_{e1} e^{j\varphi_3} e^{j\omega_0 t}) = \mathrm{Re}(\hat{F}_{e1} e^{j\omega_0 t})$ and $f_{e2}(t) = \mathrm{Re}(F_{e2} e^{j\varphi_4} e^{j\omega_0 t}) = \mathrm{Re}(\hat{F}_{e2} e^{j\omega_0 t})$, where Z_i is the displacement amplitude, and the symbol ˆ denotes the complex number.

According to the assumptions above, taking the Fourier transform of Eq. (1), we obtain

$$\begin{aligned}
&-\omega_0^2 \pi [m_1 + A_{11}(\infty)] Z_1 [e^{-j\varphi_1} \delta(\omega + \omega_0) + e^{j\varphi_1} \delta(\omega - \omega_0)] - \omega_0^2 \pi A_{12}(\infty) Z_2 [e^{-j\varphi_2} \delta(\omega + \omega_0) + e^{j\varphi_2} \delta(\omega - \omega_0)] \\
&- j\omega_0 \pi K_{11}(\omega) Z_1 [e^{-j\varphi_1} \delta(\omega + \omega_0) - e^{j\varphi_1} \delta(\omega - \omega_0)] - j\omega_0 \pi K_{12}(\omega) Z_2 [e^{-j\varphi_2} \delta(\omega + \omega_0) - e^{j\varphi_2} \delta(\omega - \omega_0)] \\
&- j\omega_0 \pi B_{vis1}(\omega) Z_1 [e^{-j\varphi_1} \delta(\omega + \omega_0) - e^{j\varphi_1} \delta(\omega - \omega_0)] + C_1 \pi Z_1 [e^{-j\varphi_1} \delta(\omega + \omega_0) + e^{j\varphi_1} \delta(\omega - \omega_0)] = \\
&F_{e1} \pi [e^{-j\varphi_3} \delta(\omega + \omega_0) + e^{j\varphi_3} \delta(\omega - \omega_0)] + F_{PTO}(\omega)
\end{aligned} \tag{5}$$

$$
\begin{aligned}
&-\omega_0^2\pi[m_2 + A_{22}(\infty)]Z_2[e^{-j\varphi_2}\delta(\omega+\omega_0) + e^{j\varphi_2}\delta(\omega-\omega_0)] - \omega_0^2\pi A_{21}(\infty)Z_1[e^{-j\varphi_1}\delta(\omega+\omega_0) + e^{j\varphi_1}\delta(\omega-\omega_0)] \\
&-j\omega_0\pi K_{22}(\omega)Z_2[e^{-j\varphi_2}\delta(\omega+\omega_0) - e^{j\varphi_2}\delta(\omega-\omega_0)] - j\omega_0\pi K_{21}(\omega)Z_1[e^{-j\varphi_1}\delta(\omega+\omega_0) - e^{j\varphi_1}\delta(\omega-\omega_0)] \\
&-j\omega_0\pi B_{vis2}(\omega)Z_2[e^{-j\varphi_2}\delta(\omega+\omega_0) - e^{j\varphi_2}\delta(\omega-\omega_0)] + (C_2 + K_m)\pi Z_2[e^{-j\varphi_2}\delta(\omega+\omega_0) + e^{j\varphi_2}\delta(\omega-\omega_0)] \\
&= F_{e2}\pi[e^{-j\varphi_4}\delta(\omega+\omega_0) + e^{j\varphi_4}\delta(\omega-\omega_0)] - F_{PTO}(\omega)
\end{aligned}
\tag{6}
$$

where

$$
\begin{aligned}
F_{PTO}(\omega) = &-K\pi\{Z_1[e^{-j\varphi_1}\delta(\omega+\omega_0) + e^{j\varphi_1}\delta(\omega-\omega_0)] - Z_2[e^{-j\varphi_2}\delta(\omega+\omega_0) + e^{j\varphi_2}\delta(\omega-\omega_0)]\} \\
&+B\omega_0\pi\{jZ_1[e^{-j\varphi_1}\delta(\omega+\omega_0) - e^{j\varphi_1}\delta(\omega-\omega_0)] - jZ_2[e^{-j\varphi_2}\delta(\omega+\omega_0) - e^{j\varphi_2}\delta(\omega-\omega_0)]\}
\end{aligned}
\tag{7}
$$

Eqs (5), (6), and (7) have the physical meaning only when $\omega=\omega_0$; thus, the hydrodynamic function set is rewritten as

$$
\begin{aligned}
&-\omega_0^2[m_1 + A_{11}(\omega_0)]\hat{Z}_1 + j\omega_0 B_{11}(\omega_0)\hat{Z}_1 + [-\omega_0^2 A_{12}(\omega_0) + j\omega_0 B_{12}(\omega)]\hat{Z}_2 \\
&+j\omega_0 B_{vis1}\hat{Z}_1 + C_1\hat{Z}_1 = \hat{F}_{e1} - K(\hat{Z}_1 - \hat{Z}_2) - j\omega_0 B(\hat{Z}_1 - \hat{Z}_2)
\end{aligned}
\tag{8}
$$

$$
\begin{aligned}
&-\omega_0^2[m_2 + A_{22}(\omega_0)]\hat{Z}_2 + j\omega_0 B_{22}(\omega_0)\hat{Z}_2 + [-\omega_0^2 A_{21}(\omega_0) + j\omega_0 B_{21}(\omega)]\hat{Z}_1 \\
&+j\omega_0 B_{vis2}\hat{Z}_2 + (C_2 + K_m)\hat{Z}_2 = \hat{F}_{e2} + K(\hat{Z}_1 - \hat{Z}_2) + j\omega_0 B(\hat{Z}_1 - \hat{Z}_2)
\end{aligned}
\tag{9}
$$

The relative displacement of the floats is expressed as $\xi(t) = z_1(t) - z_2(t)$, and its time differential is $d\xi = -\omega_0\left(u\sin\omega_0 t + v\cos\omega_0 t\right)dt$,

where $u = Z_1\cos\varphi_1 - Z_2\cos\varphi_2$ and $v = Z_1\sin\varphi_1 - Z_2\sin\varphi_2$.

Within the time interval [0, T], the average power absorption is

$$
P = -\frac{1}{T}\int_0^T f_{PTO}(t)d\xi = \frac{1}{2}B\omega_0^2\left|\hat{Z}_1 - \hat{Z}_2\right|^2 \tag{10}
$$

Further, Eqs (5) and (6) can be written as

$$
\begin{pmatrix} E_1 + j\omega_0(B + B_{11} + B_{vis1}) + K & -\omega_0^2 A_{12} - j\omega_0(B - B_{12}) - K \\ -\omega_0^2 A_{21} - j\omega_0(B - B_{21}) - K & E_2 + j\omega_0(B + B_{22} + B_{vis2}) + K \end{pmatrix} \cdot \begin{pmatrix} \hat{Z}_1 \\ \hat{Z}_2 \end{pmatrix} = \begin{pmatrix} \hat{F}_{e1} \\ \hat{F}_{e2} \end{pmatrix} \tag{11}
$$

The relative motion is calculated as

$$
\hat{Z}_1 - \hat{Z}_2 = \frac{1}{|D|}\left\{\left[-\omega_0^2 A_{21} + j\omega_0\left(B_{22} + B_{21} + B_{vis2}\right) + E_2\right]\hat{F}_{e1} + \left[\omega_0^2 A_{12} - j\omega_0\left(B_{11} + B_{12} + B_{vis1}\right) - E_1\right]\hat{F}_{e2}\right\} \tag{12}
$$

By substituting the items in Eq. (10) with the parameters defined below, the capture power can be expressed as:

$$
P = \frac{1}{2}B\omega_0^2\frac{X_1^2 + Y_1^2}{\left(P - BM\right)^2 + \left(Q - BN\right)^2} \tag{13}
$$

where

$$
D = \begin{pmatrix} E_1 + j\omega_0(B + B_{11} + B_{vis1}) + K & -\omega_0^2 A_{12} - j\omega_0(B - B_{12}) - K \\ -\omega_0^2 A_{21} - j\omega_0(B - B_{21}) - K & E_2 + j\omega_0(B + B_{22} + B_{vis2}) + K \end{pmatrix}
$$

$E_1 = -\omega_0^2(m_1 + A_{11}) + C_1$

$E_2 = -\omega_0^2(m_2 + A_{22}) + C_2 + K_m$

$\hat{F}_{ei} = F_{ei\mathrm{R}} + jF_{ei\mathrm{I}}$

$M = \omega_0 Q_K$

$N = -\omega_0 P_K$

$P = P_0 + KP_K$

$P_0 = E_1 E_2 - \omega_0^2 (B_{11} B_{22} + \omega_0^2 A_{12} A_{21} - B_{12} B_{21} + B_{11} B_{vis2} + B_{22} B_{vis1} + B_{vis1} B_{vis2})$

$P_K = -\omega_0^2 A_{12} - \omega_0^2 A_{21} + E_1 + E_2$

$Q = Q_0 + KQ_K$

$Q_0 = \omega_0 (B_{22} E_1 + B_{11} E_2 + B_{vis2} E_1 + B_{vis1} E_2 + \omega_0^2 A_{12} B_{21} + \omega_0^2 A_{21} B_{12})$

$Q_K = \omega_0 (B_{11} + B_{22} + B_{12} + B_{21} + B_{vis1} + B_{vis2})$

$X_1 = (E_2 - \omega_0^2 A_{21}) F_{e1\mathrm{R}} - \omega_0 (B_{22} + B_{21} + B_{vis2}) F_{e1\mathrm{I}} - (E_1 - \omega_0^2 A_{12}) F_{e2\mathrm{R}} + \omega_0 (B_{11} + B_{12} + B_{vis1}) F_{e2\mathrm{I}}$

$Y_1 = (E_2 - \omega_0^2 A_{21}) F_{e1\mathrm{I}} + \omega_0 (B_{22} + B_{21} + B_{vis2}) F_{e1\mathrm{R}} - (E_1 - \omega_0^2 A_{12}) F_{e2\mathrm{I}} - \omega_0 (B_{11} + B_{12} + B_{vis1}) F_{e2\mathrm{R}}$

There are some notable aspects,

(1) If K=0, the PTO force is $f_{PTO}(t) = -B(\dot{z}_1 - \dot{z}_2)$, as shown in Fig. 2. Eq. (13) is a function of only B, and the condition is called the *passive control* (Wang and Isberg, 2015). By taking the derivative of Eq. (13) with respect to B, when $\frac{\mathrm{d}P}{\mathrm{d}B} = 0$, the optimal damping coefficient is obtained, where

$$B = \sqrt{\frac{P_0^2 + Q_0^2}{M^2 + N^2}} \tag{14}$$

By substituting Eq. (14) into Eq. (13), the corresponding maximum absorption power is

$$P = \frac{1}{4}\omega_0^2 \frac{X_1^2 + Y_1^2}{\sqrt{\left(P_0^2 + Q_0^2\right)\left(M^2 + N^2\right)} - \left(P_0 M + Q_0 N\right)} \tag{15}$$

(2) If $K \neq 0$, the PTO force is determined by both the damping and stiffness coefficients, and the condition is called the *active control* (Wang and Isberg, 2015). By taking the partial differential of Eq. (13) with respect to K and B, the optimal coefficients are obtained as

$$K = -\frac{P_0 P_K + Q_0 Q_K}{P_K^2 + Q_K^2} \tag{16}$$

$$B = \sqrt{\frac{P_0^2 + Q_0^2 + \left(P_K^2 + Q_K^2\right)K^2 + 2\left(P_0 P_K + Q_0 Q_K\right)K}{M^2 + N^2}} \tag{17}$$

The maximal power capture is

$$P = -\frac{1}{8}\omega_0^2 \frac{X_1^2 + Y_1^2}{P_0 M + Q_0 N} \tag{18}$$

(3) If K in Eq. (16) is negative, it must be reset to K=0, because the negative value of K implies the use of the mechanism that is not implementable in the proposed PTO configuration (Castro and Chiang, 2020).

Fig. 2 shows the PTO force to the relative velocity of the floats under the *passive* and *active* controls.

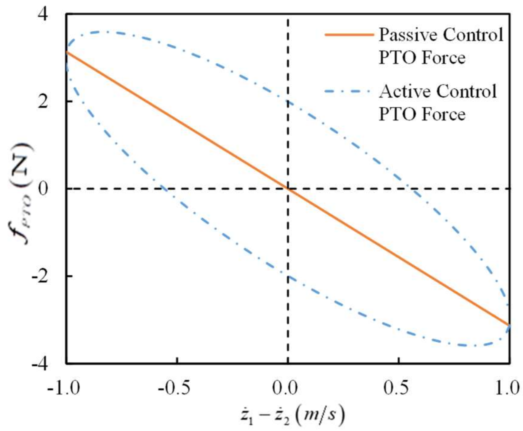

Fig. 2. Schematic of linear PTO force.

2.3 Power absorption under the constant PTO damping

When the accumulator is used in the PTO system, a constant PTO force is considered, which makes the dynamic function nonlinear. The PTO damping here can be expressed as $f_{PTO}(t) = -B\,\mathrm{sgn}(\dot{z}_1(t) - \dot{z}_2(t))$. Under the sinusoidal excitation force, the floats also respond sinusoidally with a period of $\frac{2\pi}{\omega}$, and when $\dot{z}_1(t) - \dot{z}_2(t) = 0$, the direction of the PTO force changes, as shown in Fig. 3. According to Fig. 3, the changing point can be expressed as: $t_m = -\frac{1}{\omega} arctg \frac{v}{u} + \frac{m\pi}{\omega} \quad (m = 0,1,2...)$.

In this case, the two-body heaving WEC can be analyzed numerically using the time-domain model. In contrast to the linear system, the added mass with infinite frequency, the radiation-force impulse-response function, and the excitation force in Eq. (1) can be calculated as

$$A_{iq}(\infty) = A_{iq}(\omega) + \frac{1}{\omega}\int_0^{\infty} k_{iq}(t)\sin\omega t dt \qquad (19)$$

$$k_{iq}(t) = \frac{2}{\pi}\int_0^{\infty} B_{iq}(\omega)\cos\omega t d\omega \qquad (20)$$

$$f_{ei}(t) = \int_{-\infty}^{\infty} k_{ei}(\tau)\eta(t-\tau)d\tau \qquad (21)$$

Furthermore,

$$k_{ei}(t) = \frac{1}{\pi}\int_{-\infty}^{\infty} F_{ei}(\omega)e^{j\omega t}d\omega \qquad (22)$$

The average power absorption can be calculated by the integration,

$$P = -\frac{1}{T}\int_0^{T} f_{PTO}(t)\left[\dot{z}_1(t) - \dot{z}_2(t)\right]dt \qquad (23)$$

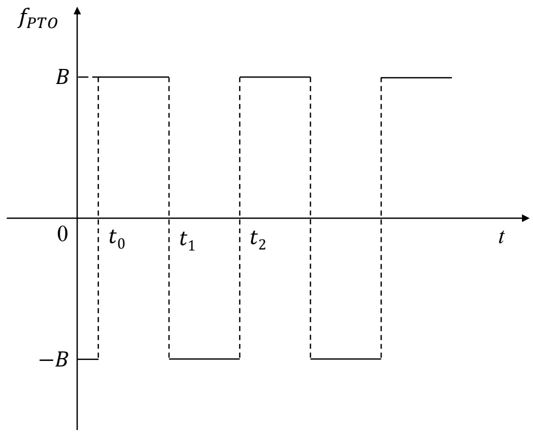

Fig. 3. Schematic of the constant PTO damping.

2.4 Model validation

To validate the analysis of both linear and constant PTO damping forces in this study, the results are compared with those obtained in other research. For the linear PTO condition, the configuration of the model-scaled two-body WEC is cited from Wang et al. (2016), as shown in Fig. 4, and the specific parameters are listed in Table 1. Viscous damping was considered in reference. For the outer float, viscous damping was determined by the experiment conducted by Son and Yeung (2014). For the inner float, Wang et al. (2016) referred to the data of Tom and Yeung (2013) to investigate the viscous effects. Two cases were computed and compared for regular waves. One is 1 DOF, which means that only the outer float can move and the inner float is a fixed cylinder. The other is 2 DOF, which allows both floats to move independently and simultaneously. The hydrodynamic coefficients are solved by the method of matched eigenfunction expansions, and the results of Wang et al. (2016) are derived in the frequency domain. A comparison of the CWR with viscous damping between the reference and present studies under different DOFs is shown in Fig. 5. It can be seen from Fig. 5 that the dynamic analysis in this study can be validated by Wang's results. For the constant PTO, the verified full-scaled WEC is Wavebob, as shown in Fig. 6, with the parameters listed in Table 2. Kalidoss and Banerjee (2019) calculated the power absorption of Wavebob with different piston areas. The PTO force is defined as the product of the piston area of the hydraulic cylinder and the pressure difference between the high-pressure and low-pressure accumulators. The hydrodynamic coefficients of Wavabob were calculated using WAMIT. When modeling the power absorption of the WEC, SIMULINK was used, and the multi-body interaction of the WEC was solved in WEC-Sim. The wave condition of the simulation is a regular wave with a wave height of 5.5 m and wave period of 7.0 s. The simulation was run for approximately 72 wave periods to obtain a steady-state solution. Fig. 7 shows a comparison between the results of Kalidoss and Banerjee (2019) and those of this study. Thus, the present study could be validated.

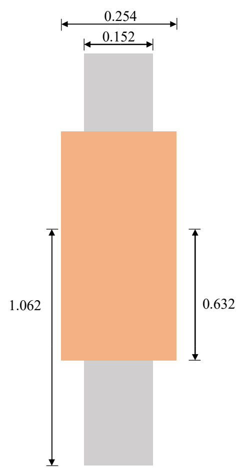

Fig. 4. WEC for validation of the model with linear PTO damping force (Wang et al., 2016).

Table 1 Geometric parameters of the verified WEC

Property	Value
Inner cylinder radius (m)	0.152
Outer cylinder radius (m)	0.254
Inner cylinder draft (m)	1.062
Outer cylinder draft (m)	0.632
Water depth (m)	1.524

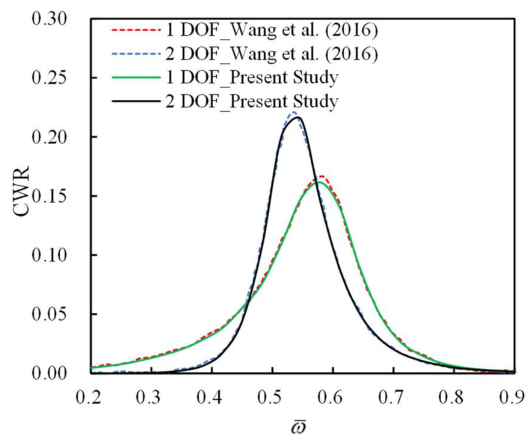

Fig. 5. Comparison of Wang et al.'s and the present study on the CWR.

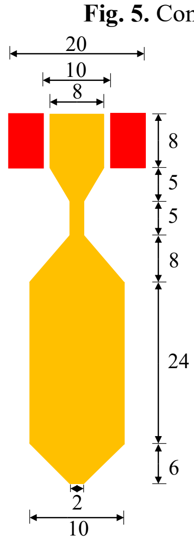

Fig. 6. WEC for validation of the model with constant PTO damping force (Kalidoss and Banerjee, 2019).

Table 2 Main parameters of the verified WEC

Property	Torus	Spar
Mass (t)	278	4680
Radius (m)	5/10	8 (at the mean water lever, MWL)
Length (m)	8	56
Draft (m)	2	50
Centre of mass (m)	0	-35
Ixx (t • m^2)	12400	1740000
Iyy (t • m^2)	12400	1740000
Izz (t • m^2)	16500	1510000

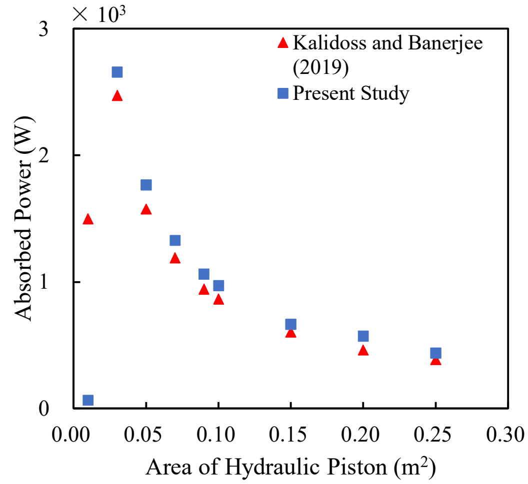

Fig. 7. Validation of the present model for power absorption by the PTO system.

3 Power capture performance

A specified two-body heaving WEC with the geometric parameters listed in Table 3 is used in the model analysis. All the variables used in this paper are nondimensionalized in Table 4. The definitions of the parameters used in Tables 3 and 4 can be found in Section 2.

Table 3 Geometric parameters of the model

Variable	Symbol	Quantity	Unit
Outer radius of outer float	R_1	40.00	cm
Inner radius of outer float	r_1	20.00	cm
Radius of inner float	R_2	18.00	cm
Draft of the outer float	D_1	15.50	cm
Draft of the inner float	D_2	70.00	cm

Table 4 List of non-dimensional variables

Variable	Dimensional variable symbol	Dimensional variable unit	Non-dimensional variable symbol	Definition of the non-dimensional variabe
Wave frequency	ω	rad/s	ϖ	$\varpi = \omega / \sqrt{g/R_1}$
Added mass	A_{iq}	kg	$\bar{A}_{iq}$	$\bar{A}_{iq} = A_{iq} / \pi\rho R_1^3$
Radiation damping	B_{iq}	kg/s	$\bar{B}_{iq}$	$\bar{B}_{iq} = B_{iq} / \pi\rho\omega R_1^3$
Linear PTO damping coefficient	B	kg/s	$\bar{B}$	$\bar{B} = B / \pi\rho g^{1/2} R_1^{5/2}$
Linear PTO stiffness coefficient	K	kg/s^2	$\bar{K}$	$\bar{K} = K / \pi\rho g R_1^2$
Constant PTO damping force	F_{PTO}	N	$\bar{F}_{PTO}$	$\bar{F}_{PTO} = F_{PTO} / \rho\omega^2 R_1^3 H$

3.1 Power absorption under different PTOs

Three different PTO damping forces are considered, namely, the aforementioned passive and active-controlled linear PTOs, and the constant PTO. The heave motion response amplitude operator (RAO) of the WEC's free oscillation is discussed in advance. The heave motion RAO, which is defined as the amplitude of the body's heave displacement, normalized by the wave amplitude, is used to evaluate the hydrodynamic performance of the two-body heaving WEC. The RAOs of the floats without PTO and the incoming wave power per unit width of the wave front are shown in Fig. 8. As shown in Fig. 8, the heave motion RAO of the relative motion has two distinct peaks, which are located around the natural frequencies of the outer ($\overline{\varpi} = 1.14$) and inner ($\overline{\varpi} = 0.70$) floats. In addition, the curve implies a better capture performance of the two-body system than the single-body system, because of the wider resonance range.

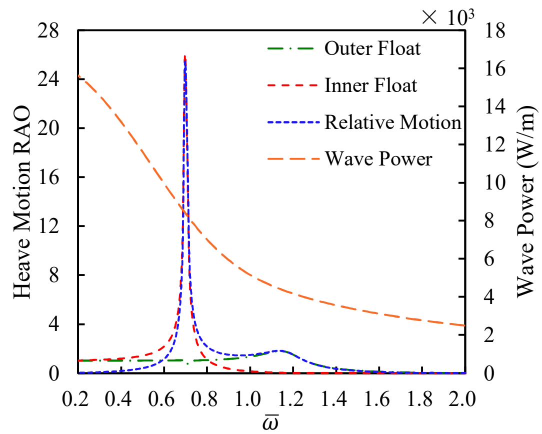

Fig. 8. Heaving motion RAO and wave power of the two-body heaving WEC.

During the numerical modeling of the WEC with the passive-controlled linear PTO, $\overline{\varpi}$ takes the value of 0.60~1.40 with an interval of 0.20. In particular, as shown in the curve of RAO, a local refinement is performed at around 0.70, adding three frequencies of 0.65, 0.70, and 0.75. The trends of the CWR and heave motion RAO against the damping coefficient $\overline{B}$ are shown in Fig. 9. This shows that the CWR increases first and then decreases with an increase in $\overline{B}$. The optimal CWR and corresponding $\overline{B}$ values vary with $\overline{\varpi}$. When $\overline{\varpi}$=0.70 , the CWR of the WEC reaches a peak value at a small damping, and the curve is narrow. However, when $\overline{\varpi}$=1.00 , the WEC performs better at most of the damping force. The relative heave motion RAO keeps dropping down against $\overline{B}$, which is well understood because the larger the damping is, the more the relative motion between the two floats tends to be together. The rate of decline is the largest when $\overline{\varpi}$=0.70 , which indicates that the relative motion of the device is most sensitive to the influence of $\overline{B}$ at this frequency.

When the active-controlled linear PTO is applied, the damping coefficient $\overline{B}$ is fixed at 0.098. Fig. 10 shows the trends of the CWR and heave motion RAO with the non-dimensional stiffness coefficient $\overline{K}$. Evidently, the CWR increases up to a peak value with $\overline{K}$ and then decreases. The heave motion RAO is almost the same as that of CWR, with one exception when $\overline{\varpi} < 0.70$, and the reason is explained in Section 3.2. It is easier to adjust the stiffness coefficient than the damping coefficient of the device, making it well responsive to the incident wave frequency; however, the damping part of the PTO is still a dominant factor in the power absorption. To explore the relationship between the stiffness and damping coefficients, Fig. 11 shows the features of the CWR and RAO with respect to the stiffness coefficient under different damping forces. Here, $\overline{\varpi}$ is 0.8 and 1.0. This reveals that the trends of CWR and RAO with the consideration of stiffness coefficient do not change with the damping coefficient. Hence, the optimal values can be obtained separately. Furthermore, the optimal stiffness coefficient remains unchanged against different damping coefficients; therefore, it only depends on the wave frequency.

The CWR and RAO of the WEC for a constant PTO damping force are plotted in Fig. 12. It shows that the CWR increases first, then keeps a downward tendency, and approaches zero until the PTO force makes the two floats move together. In terms of the RAO, the motion response of the WEC declines with an increase in the PTO force.

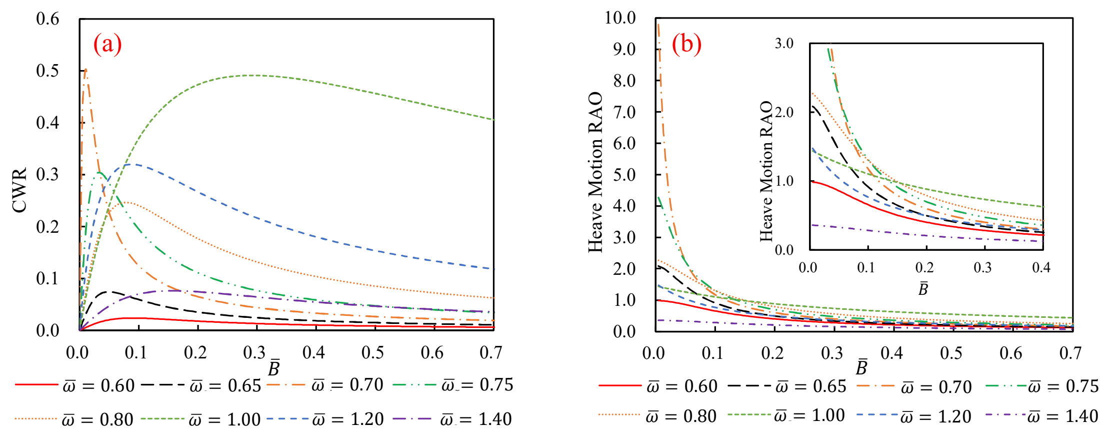

Fig. 9. CWR (a) and RAO (b) of the WEC under the passive-controlled linear PTO.

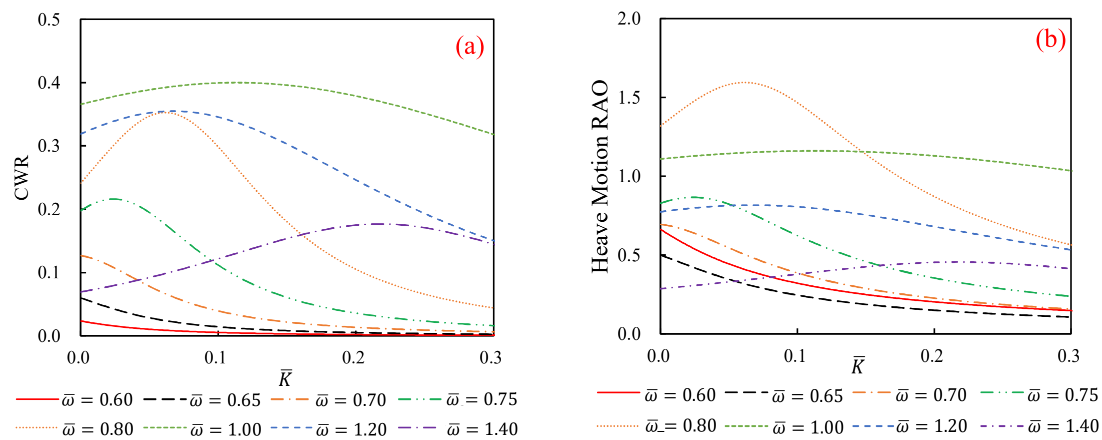

Fig. 10. CWR (a) and RAO (b) of the WEC under the active-controlled linear PTO.

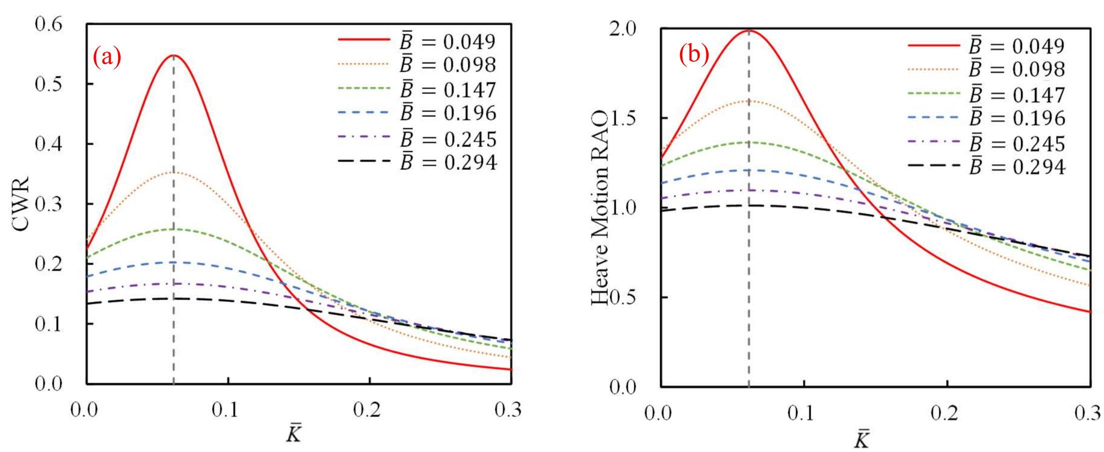

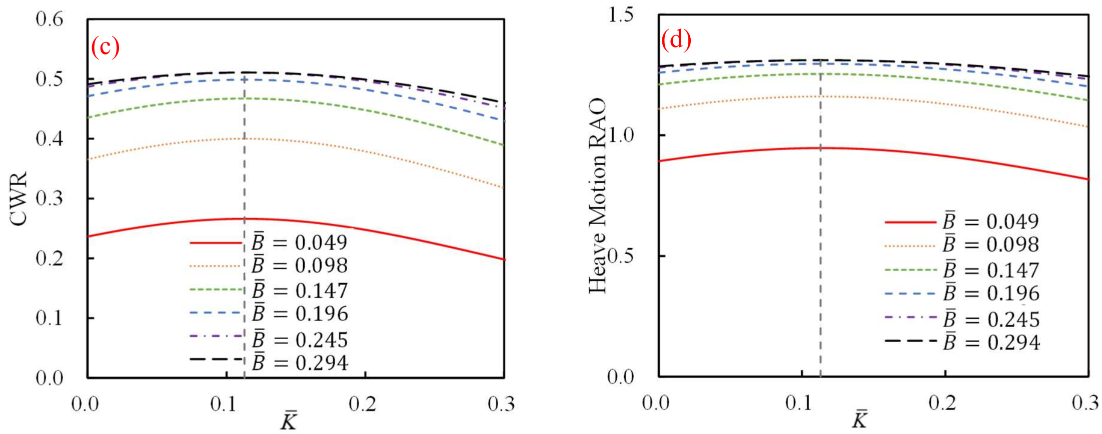

Fig. 11. CWR and RAO of the WEC against $\bar{K}$ with different B when $\bar{\omega}$ is (a), (b) 0.8, and (c), (d) 1.0.

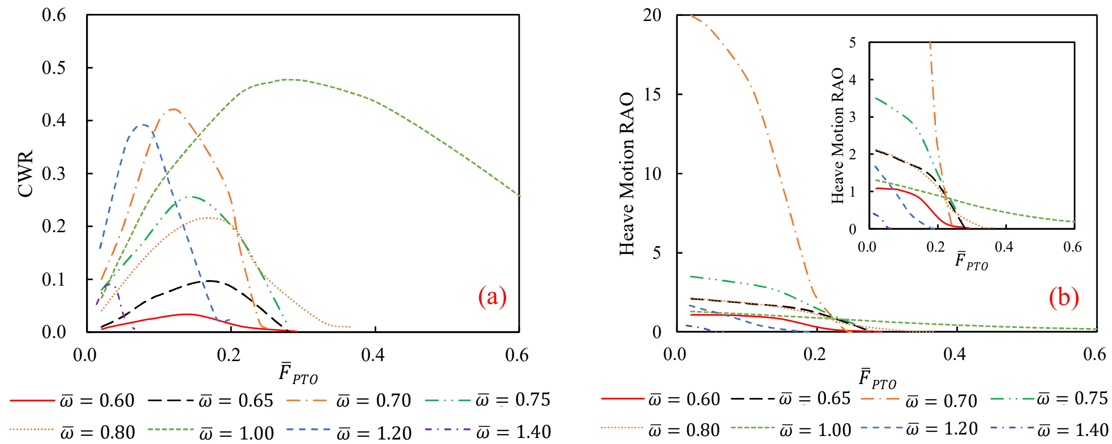

Fig. 12. CWR (a) and RAO (b) of the WEC under the constant PTO.

3.2 Optimal PTO parameters

Four cases are presented here to show the optimal PTO parameters and power absorption performance of the two-body heaving WEC. The model provides one *comparison case*, where the inner float is fixed to unmovable, and under which the mooring stiffness is infinite. The comparison case is the baseline case, and the remaining cases correspond to the three PTO forces in Section 2. Descriptions of the four cases are listed in Table 5. The optimal non-dimensional PTO parameter as a function of the non-dimensional frequency is shown in Fig. 13a, while the corresponding optimal CWR is shown in Fig. 13b.

The optimal coefficients are determined in two different ways. One is to apply Eqs (14), (16), and (17). The other is to sweep through these coefficients from zero to a large value. As shown in Fig. 13a, the damping coefficient has two overlapping parts under passive and active control. One occurs when the wave frequency is smaller than the natural frequency of the inner float, while the other occurs at the natural frequency of the outer float. The reason for the former is the manual zeroing of the stiffness coefficient to avoid a negative value. The latter is because the WEC has already resonated with waves, and the stiffness coefficient is sufficiently small. This also explains why the CWR monotonically decreases with $\bar{K}$ when $\bar{\omega}$<0.7 , as in that case, the optimal stiffness coefficient is modulated to zero by artificial correction. The optimal constant PTO force exhibits a trend similar to the damping coefficient of the passive control. Evidently, the WEC responds strongly when the incident wave frequency is between the natural frequencies of the two floats, and conquers as large PTO damping force as possible.

For the passive control linear PTO and constant PTO conditions, two well-separated peaks in the CWR are observed, as shown in Fig. 13b. The low-frequency peak is near the natural frequency of the inner float, and the high-frequency peak is near that of the outer float, whereas in the active control PTO condition and the comparison case, only one peak appears. In fact, the peak under the active control condition could be treated as the merging of peaks in the passive condition, because it is located between the natural frequencies of the floats. This also implies that the WEC can be in tune with the wave by adjusting the stiffness part of the PTO system. In the comparison case, only one peak is observed at the natural frequency of the outer float. In other words, the two-body heaving WEC always has more opportunities than a single float.

Table 5 Description of four cases

Case	DOF of inner float	PTO force	Composition of PTO force
Passive control	Free	Linear	Damping part
Active control	Free	Linear	Damping and stiffness part
Comparison case	Fixed	Linear	Damping part
Constant PTO force	Free	Constant	Damping part

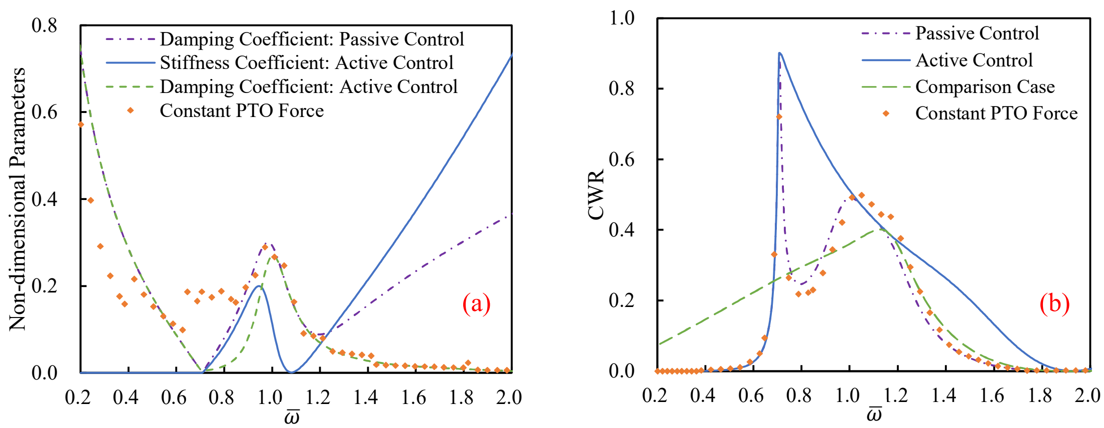

Fig. 13. Optimal PTO parameters (a) and the CWR (b) against non-dimensional wave frequency.

4 Estimation of the optimal power absorption

For a WEC with certain geometric parameters, the optimal power absorption is determined by the PTO damping when the wave condition is given. Viscous effects are not included in the above discussion. Therefore, smaller dynamic response and power absorption should be expected in a real case when viscous damping is considered. The viscous damping coefficient can be used and obtained by the physical model test; here, the data of Dong et al. (2021) are used to verify the correction of the heave motion RAO and power absorption. Four different cases are shown in Fig. 14, and the differences of the four cases are listed in Table 6. When there is no viscous damping applied on the WEC, the heave motion RAO and CWR has two distinct peaks, which are discussed in Section 3. In this situation, the high heave motion RAO and CWR attract attention. Consequently, the viscous damping is considered in the computation. The ratio of the linearized viscous damping to the radiation damping is determined by free decay test. It is observed that the peak value around the inner float decreases sharply when the viscous damping of the inner float applied, but the heave motion RAO still has two peaks. Furthermore, when both floats are applied viscous damping, only one peak occurs in heave motion RAO and CWR, which proves the expected point. The numerical results are also compared with the experimental results, and the results are in good agreement. This shows that the existence of the viscosity makes one of the peaks disappear, which is compared to the two peak values in the absence of viscous damping in Section 3, and the power absorption reduces sharply.

Table 6 Difference of four cases

Case	Viscous damping of outer float	Viscous damping of inner float	Method
Dong et al. (2021)	√	√	Experimental (Heave motion RAO) Numerical (CWR)
No viscous damping	×	×	Numerical
Viscous damping of inner float	×	√	Numerical
Viscous damping of two floats	√	√	Numerical

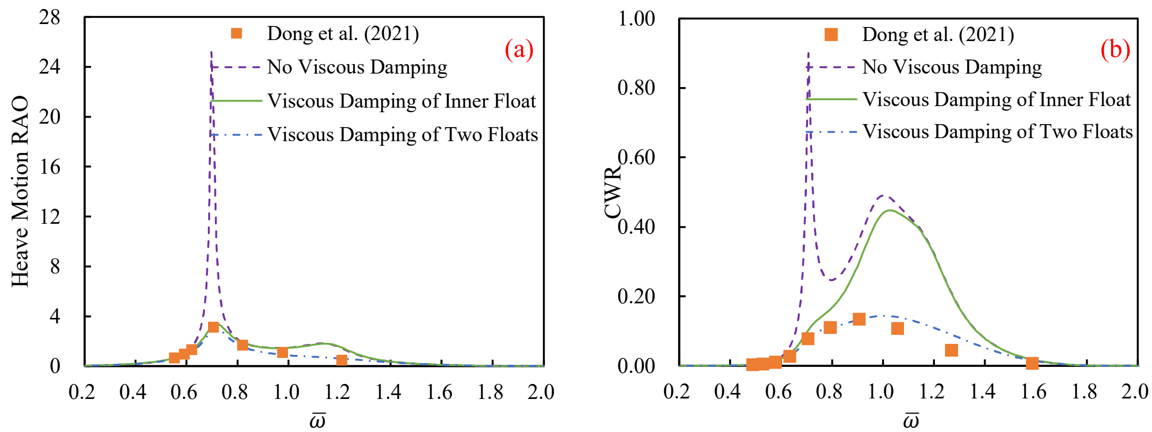

Fig. 14. Comparison of the heave motion RAO (a) and CWR (b) with different viscous damping conditions.

The derivation of the optimal power absorption of the device is complex and time-consuming, especially in reality. Here, a new estimation formula called the PCF is constructed to provide an efficient and convenient way of predicting power absorption. Obviously, when the PTO damping force is 0, the power capture of the WEC is 0. When the PTO damping force increases to a value that makes the floats with NO relative motion, the power capture is also 0. In addition, the higher the incident wave amplitude is, the more power the WEC captures. Therefore, inspired by Eq. (13), a function such as Eq. (24) is constructed to estimate the average power absorption of the two-body heaving WEC.

$$P = \alpha \omega_0^2 A^2 \frac{B}{B^2 + \beta B + \gamma} \tag{24}$$

where α, β, and γ are the unknown coefficients related to the WEC feature, B is the linear PTO damping coefficient or the constant PTO damping force, ω_0 is the incident wave frequency, and A is the incident wave amplitude.

From Eq. (24), it can be seen that the power absorption of the WEC first increases and then decreases with an increase in B (as shown in Fig. 15), which is in line with the above analysis results. The optimal PTO damping coefficient or force occurs when $B = \sqrt{\gamma}$, and the optimal power of the WEC can be predicted as

$$P = \alpha \omega_0^2 A^2 \frac{1}{\beta + 2\sqrt{\gamma}} \tag{25}$$

Eq. (25) is a general expression of the absorption power, which considers all aspects, such as viscosity and friction. It is suitable for different kinds of PTOs whatever linear or constant. The unknown coefficients can be obtained by a model test or numerical simulation in a few cases. The specific method is described below.

Three different values of PTO damping forces are chosen in the model test or numerical simulation under the same incident wave condition; thus, three sets of PTO damping coefficients or forces (B_1, B_2, and B_3) and the corresponding captured power (P_1, P_2, and P_3) can be derived. The above three sets of data are introduced into Eq. (26) to obtain the unknown coefficients α, β, and γ. Then, these three unknown coefficients are substituted into Eq. (25) to obtain the optimal power absorption of the WEC under wave conditions.

$$\begin{cases} \alpha = \dfrac{B_1 + \beta + \dfrac{\gamma}{B_1}}{\omega_0^2 A^2} P_1 \\ \beta = \dfrac{B_2 B_3 \left(B_2 P_2 - B_3 P_3\right) + \left(B_3 P_2 - B_2 P_3\right)\gamma}{B_2 B_3 \left(P_3 - P_2\right)} \\ \gamma = \dfrac{B_1 B_3 \left[B_2 \left(P_3 - P_2\right)\left(B_2 P_2 - B_1 P_1\right) + B_2 \left(B_2 P_2 - B_3 P_3\right)\left(P_2 - P_1\right)\right]}{B_3 \left(P_3 - P_2\right)\left(B_2 P_1 - B_1 P_2\right) + B_1 \left(P_1 - P_2\right)\left(B_3 P_2 - B_2 P_3\right)} \end{cases} \tag{26}$$

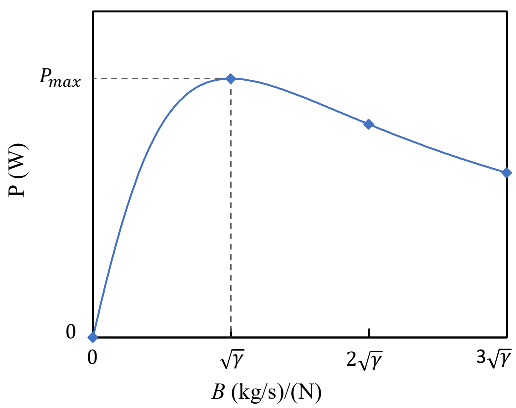

Fig. 15. Power absorption against PTO damping coefficient (for linear) or force (for constant) in estimation formula.

To validate the above method, a model test of the WEC with the parameters listed in Table 3 and constant PTO damping was conducted. The model test was set up at the Shandong Provincial Key Laboratory of Ocean Engineering. The wave tank is 60 m long, 36 m wide, and 1.5 m deep. A piston-type wave maker is featured in the front of the wave tank, which can generate waves with heights ranging from 0.05 m to 0.25 m, and periods ranging from 0.5 s to 2.5 s in both regular and irregular wave conditions. The water depth of the model test was 1.1 m, and the model WEC was placed 30 m from the wave maker and 7 m from one side of the flanks to diminish the wall effect. By considering the capacity of the wave tank, the inherent performance of the WEC, and the wave condition of the target sea area, the model test selects the wave conditions with a wave height range between 7.5 and 20.0 cm, and a wave period range between 1.05 and 2.30 s (Dong et al., 2021). In the model test, a specific hydraulic system was applied to provide a constant PTO damping force by adjusting the pressure. The outer float is connected to the piston rod of the hydraulic cylinder, and the inner float is connected to the hydraulic cylinder body. The volumes of the upper and lower chambers of the hydraulic cylinder varied with the relative motion of the two floats. When the piston is upward relative to the initial position, the upper chamber pressure is larger than the lower one, and the outer float is subjected to a downward damping force, whereas the inner float is subjected to a force in the opposite direction, and vice versa. The hydraulic system controls the pressure difference between the chambers by adjusting the proportional solenoid relief valve so that the PTO damping force acting on the floats can be controlled. Through the closed-loop system, the PTO force provided by the hydraulic system can meet the requirement. To compare the optimal power absorption between the estimated and experimental values under different wave conditions, five typical cases are listed in Table 7, which cover different wave heights, wave periods, and mass ratios. The data are compared with the estimated values as shown in Fig. 16a, and the average error is 3%. Furthermore, the numerical simulation data from Dong et al. (2021) are also used for the comparison with the estimated values, under the incident wave conditions of wave amplitude A=0.05 m, period T=1.0~2.0 s in a group interval of 0.2 s, as shown in Fig. 16b. The numerical model has already been validated by the model test, and the linear PTO damping force is applied to the two-body WEC instead of the constant PTO damping force. The simulation data were obtained by using the boundary element method, and the optimal values were obtained by sweeping. The average error between the numerical simulation and PCF is approximately zero. Therefore, the validations can prove that the PCF is convincing in predicting the WEC's power absorption with different kinds of PTO damping forces.

To further verify the correctness of the PCF, the data from Tan et al. (2020) were selected for reference. The subject to be studied is a two-body WEC with a damping plate connected to the inner float, and the energy capture was simulated by introducing a linearized force in the frequency domain. Tan et al. (2020) employed a slotless Halbach linear generator as the PTO system and linearized the nonlinear time domain into a frequency domain to simulate the linear PTO damping force on the WEC. The PCF selects three sets of simulation results to estimate the optimal power absorption at each wave frequency. Fig. 17a shows that the estimated optimal capture power is in good agreement with the reference value at different wave frequencies (from 1 to 5 rad/s) with an average error of 5%. Jin et al. (2019) proposed a coaxial-cylinder WEC, and the optimization of a coaxial-cylinder WEC through actively controlled generator damping and stiffness was studied numerically. The radii of the outer and inner cylinders are 0.25 m and 0.15 m, respectively, and the drafts of the outer and inner cylinders are 1.0 m and 0.6 m, respectively. The water depth was set as 2.0 m. The results of the PCF are compared with the data presented in the reference, as shown in Fig. 17b. Here, consistent with the reference, the CWR is illustrated instead of the optimal power. The average error of these six cases is 9%. Based on the above study, the capability of the PCF has been proved. The PCF can quickly estimate the optimal power of the WEC under various conditions, covering different PTO schemes and research methods.

Table 7 Compared case conditions

Case	Incident wave height (cm)	Incident wave period (s)	Mass ratio between the outer and inner floats
1	17.5	1.30	0.84
2	17.5	1.55	0.84
3	17.5	1.80	0.84
4	20.0	1.80	0.84
5	20.0	1.80	1.17

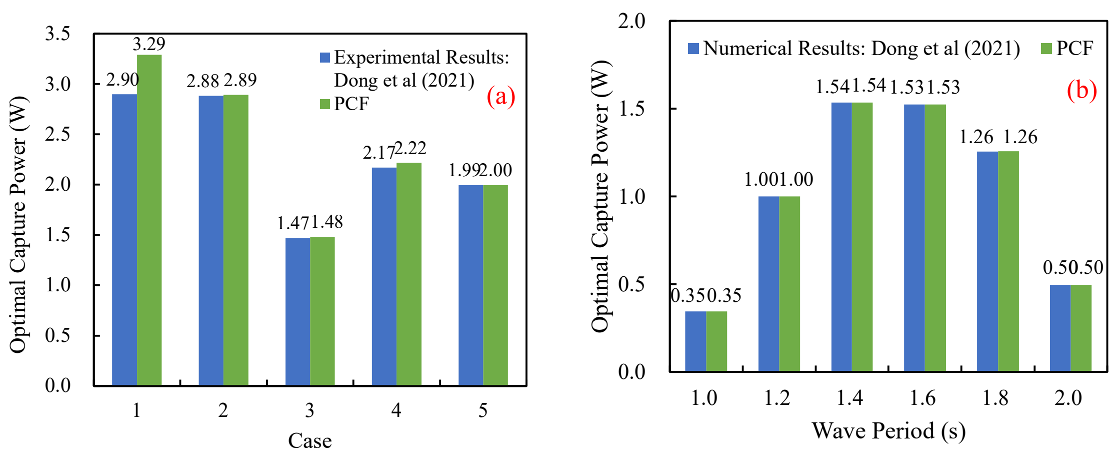

Fig. 16. Comparisons of the optimal power absorption between the PCF and the experimental results (a) and the

numerical results (b).

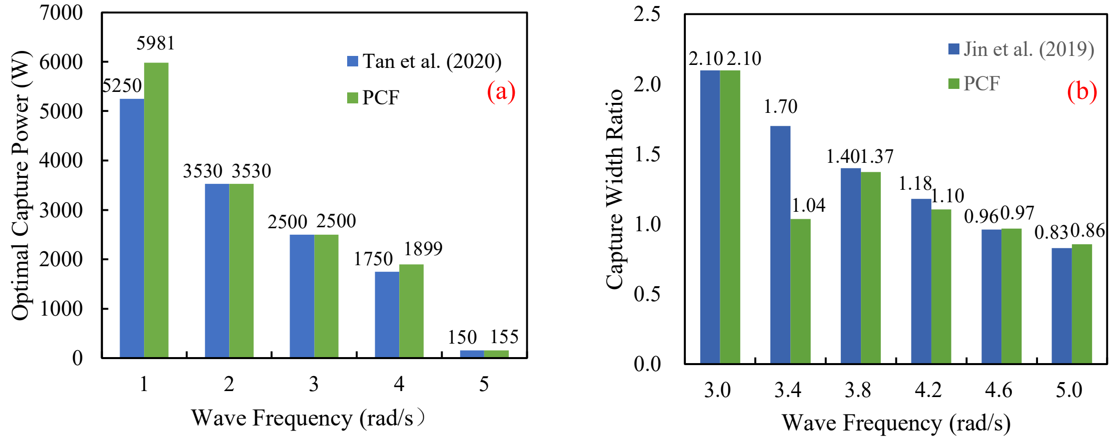

Fig. 17. Comparison of the optimal power absorption between the PCF and Tan et al.'s (a) and Jin et al.'s (b) studies.

5 Conclusions

Based on the classical potential flow theory, this study establishes a hydrodynamic analysis model of a two-body heaving WEC, describing the relative motion of the floats, through which the conversion mechanism is revealed analytically and numerically. According to the control function and the necessary conditions, the optimal PTO damping coefficient and maximum power absorption are solved under the linear and constant PTO hypotheses. A semi-experienced formula (PCF) is given to estimate the maximum power absorption under the optimum PTO damping force. The results presented are important in WEC design.

(1) The two-body heaving WEC typically has two distinct resonant frequencies; therefore, a proper design with optimal PTO damping can achieve a better power capture performance than the single-body WEC.

(2) The PTO scheme of the active control can enhance the poorly performing part of the passive control, and makes the WEC be in tune with the incident wave to obtain the optimal power. The stiffness and damping coefficients of the PTO damping force are decoupled and can be optimized separately.

(3) The new PCF formula, which is proposed for estimating optimal power, is reasonable and easy to use. Only a few sets of tests are required to solve the parameters and adapt to different PTO damping forces, so that the actual optimal power absorption of the device can be estimated efficiently.

In this study, inviscid conditions are to reveal the characteristics of the motion response and power absorption of the two-body heaving WEC under different PTO systems, which is the main purpose. Viscid conditions are discussed to verify the correctness of the analysis and show the effect of viscous damping on the performance of the WEC. In the future, the study will focus on the optimization of the WEC under the effect of viscous damping and mooring system.

Acknowledgements

This work was supported by the National Key R&D Program of China (Grant No.: 2018YFB1501904), the Shandong Provincial Key R&D Program (Grant NO.: 2019JZZY010902), the National Natural Science Foundation of China (Grant No.: 52071303), the Joint Project of NSFC-SD (Grant No. U1906228), and the Taishan Scholars Program of Shandong Province(No. ts20190914).

References

Al Shami, E., Wang, X. and Ji, X.Y., 2019. A study of the effects of increasing the degrees of freedom of a point-absorber wave energy converter on its harvesting performance, *Mechanical Systems and Signal Processing*, 133, 1-26.

Amann, K.U., Magaña, M.E. and Sawodny, O., 2015. Model predictive control of a nonlinear 2-body point absorber wave energy converter with estimated state feedback, *IEEE Transactions on Sustainable Energy*, 6(2), 336-345.

Beatty, S.J., Bocking, B.J., Bubbar, K., Buckham, B.J. and Wild, P., 2019. Experimental and numerical comparisons of self-reacting point absorber wave energy converters in irregular waves, *Ocean Engineering*, 173, 716-731.

Berenjkoob, M.N., Ghiasi, M. and Soares, C.G., 2019a. On the improved design of the buoy geometry on a two-body wave energy converter model, *Journal of Renewable and Sustainable Energy*, 11(5), 1-13.

Berenjkoob, M.N., Ghiasi, M. and Soares, C.G., 2019b. Performance of two types of mooring systems in the heave motion of a two-body floating wave energy converter, *Journal of Marine Science and Application*, 18:38~47.

Blanco, M., Lafoz, M., Ramirez, D., Navarro, G., Torres, J. and Garcia, T.L., 2019. Dimensioning of point absorbers for wave energy conversion by means of differential evolutionary algorithms, *IEEE Transactions on Sustainable Energy*, 10(3), 1076-1085.

Castro, F.A. and Chiang, L.E., 2020. Design optimization and experimental validation of a two-body wave energy converter with adjustable power take-off parameters, *Energy for Sustainable Development*, 56, 19-32.

Chau, F.P. and Yeung, R.W., 2012. Inertia, damping, and wave excitation of heaving coaxial cylinders, *Proceedings, 31st ASME International Conference on Ocean, Offshore and Arctic Engineering*, Rio de Janeiro, Brazil, 803-813.

Chen, H., Qian, L., Ma, Z.H., Bai, W., Li, Y., Causon, D. and Mingham, C., 2019. Application of an overset mesh based numerical wave tank for modelling realistic free-surface hydrodynamic problems, *Ocean Engineering*, 176, 97-117.

Dai, Y.M., Chen, Y.Z. and Xie, L.H., 2017. A study on a novel two-body floating wave energy converter, *Ocean Engineering*, 130, 407-416.

Dong, X.C., Gao, Z., Li, D.M. and Shi, H.D., 2021. Experimental and numerical study of a two-body heaving wave energy converter with different power take-off models, *Ocean Engineering*, 220, 1-22.

Elwood, D., Yim, S.C., Prudell, J., Stillinger, C., Jouanne, A.V, Brekken, T., Brown, A. and Paasch, R., 2010. Design, construction, and ocean testing of a taut-moored dual-body wave energy converter with a linear generator power take-off, *Renewable Energy*, 35(2), 348-354.

Huang, L., Hu, B.B., Hu, M.Q., Liu, C.Y. and Zhu, H., 2019. Research on primary excitation fully superconducting linear generators for wave energy conversion, *IEEE Transactions on Applied Superconductivity*, 29(5), 1-5.

Ji, R.W., Sheng, Q.H., Wang, S.Q., Zhang, Y.Q., Zhang, X.W. and Zhang, L., 2019. Array characteristics of oscillating-buoy two-floating-body wave-energy converter, *Journal of Marine Science and Application*, 18(03), 325-333.

Ji, X.Y, Shami, E.A., Monty, J. and Wang, X., 2020. Modelling of linear and non-linear two-body wave energy converters under regular and irregular wave conditions, *Renewable Energy*, 147, 487-501.

Jin, P., Zhou, B.Z., Goteman, M., Chen, Z.F. and Zhang, L., 2019. Performance optimization of a coaxial-cylinder wave energy converter, *Energy*, 174, 450-459.

Kalidoss, S. and Banerjee, A., 2019. Performance evaluation of floating two-body wave energy converter with hydraulic power take-off system, *Proceedings of the Fourth International Conference in Ocean Engineering (ICOE2018)*, Singapore, Singapore, 883-897.

Kurniawan, A., Grassow, M. and Ferri, F., 2019. Numerical modelling and wave tank testing of a self-reacting two-body wave energy device, *Ships and Offshore Structures*, 14, 344-356.

Lewis, T.M., Jouanne, A.V. and Brekken, T.K.A., 2012. Modeling and control of a slack-moored two-body wave energy converter with finite element analysis, *Energy Conversion Congress and Exposition (ECCE),* Raleigh, NC, USA, 938-945.

Liang, C.W. and Zuo, L., 2017. On the dynamics and design of a two-body wave energy converter, *Renewable Energy*, 101, 265–274.

Mavrakos, S. A., 2004. Hydrodynamic coefficients in heave of two concentric surface-piercing truncated circular cylinders, *Applied Ocean Research*, 26(3-4), 84-97.

Negandari, M., Dalayeli, H. and Moghadas, M.H., 2018. Design of a two-body wave energy converter by incorporating the effect of hydraulic power take-off parameters, *Journal of Marine Science and Technology*, 26(4), 496-507.

Phung, V.N., Nguyen, T.M., Dang, T.B. and Phan, D.T., 2019. Numerical simulation of a wave energy converter using linear generator, *Proceedings of the 1st Vietnam Symposium on Advances in Offshore Engineering. VSOE. Lecture Notes in Civil Engineering,* Springer, Singapore, 18, 319-326.

Son, D., Belissen, V. and Yeung, R.W., 2016. Performance validation and optimization of a dual coaxial cylinder ocean-wave energy extractor, *Renewable Energy*, 92, 192-201.

Son, D. and Yeung, R. W., 2014. Performance predictions and validation of a two coaxial-cylinder system as a wave energy extractor, *Proceedings of the ASME 2014 33rd International Conference on Ocean, Offshore and Arctic Engineering*, San Francisco, USA, 1-10.

Tan, Y.M., Liu, N., Lin, K.J. and Zhang, Z.G., 2020. Frequency domain modeling of a halbach pm linear generator based two-body point absorber for wave energy conversion, *Frontiers in Energy Research*, 8, 1-16.

Tom, N. and Yeung, R. W., 2013. Performance enhancements and validations of a generic ocean-wave energy extractor, *Journal of Offshore Mechanics and Arctic Engineering*, 135(4), 1-10.

Wang, L., Son, D. and Yeung, R.W., 2016. On the performance of a dual-cylinder wave-energy converter: single versus two degrees of freedom, *Proceedings of the ASME 2016 35th International Conference on Ocean, Offshore and Arctic Engineering*, Busan, South Korea, 1-9.

Wang, L.G. and Isberg, J., 2015. Nonlinear passive control of a wave energy converter subject to constraints in irregular waves, *Energies*, 8(7), 6528-6542.

Xu, Q.L., Li, Y., Yu, Y.H., Ding, B.Y., Jiang, Z.Y., Lin, Z.L. and Cazzolato, B., 2019. Experimental and numerical investigations of a two-body floating-point absorber wave energy converter in regular waves, *Journal of Fluids and Structures*, 91, 1-19.

Yang, S.H., Ringsberg, J.W., Johnson, E., Hu, Z.Q., Bergdahl, L. and Duan, F., 2018. Experimental and numerical investigation of a taut-moored wave energy converter: a validation of simulated buoy motions, *Proceedings of the Institution of Mechanical Engineers Part M-Journal of Engineering for the Maritime Environment*, 232 (1), 97-115.

Yu, Y.H. and Li, Y., 2013. Reynolds-averaged navier-stokes simulation of the heave performance of a two-body floating-point absorber wave energy system, *Computers and Fluids*, 73, 104-114.

Zhang, L., Jin, P., Zhou, B.Z., Zheng, X. and Liu, H., 2019. Oscillation and conversion performance of double-float wave energy converter, *Journal of Marine Science and Application*, 18(001), 54-63.